A Holistic State Estimation Framework for Active Distribution Network with Battery Energy Storage System

Shaojian Song, *Member*, *IEEE*, Huangjiao Wei, Yuzhang Lin, *Member*, *IEEE*, Cheng Wang, *Member*, *IEEE*, and Antonio Gómez-Expósito, *Fellow*, *IEEE*

Abstract—Battery energy storage systems (BESSs) are expected to play a crucial role in the operation and control of active distribution networks (ADNs). In this paper, a holistic state estimation framework is developed for ADNs with BESSs integrated. A dynamic equivalent model of BESS is developed, and the state transition and measurement equations are derived. Based on the equivalence between the correction stage of the iterated extended Kalman filter (IEKF) and the weighted least squares (WLS) regression, a holistic state estimation framework is proposed to capture the static state variables of ADNs and the dynamic state variables of BESSs, especially the state of charge (SOC). A bad data processing method is also presented. The simulation results show that the proposed holistic state estimation framework improves the accuracy of state estimation as well as the capability of bad data detection for both ADNs and BESSs, providing comprehensive situational awareness for the whole system.

Index Terms—Active distribution network (ADN), anomaly detection, battery energy storage system (BESS), Kalman filtering, situational awareness, state estimation, state of charge (SOC).

I. INTRODUCTION

DUE to the integration of distributed generators (DGs), energy storage systems, electric vehicles, and controllable loads, distribution networks are gradually becoming active distribution networks (ADNs), where the traditional operation and control paradigm is no longer applicable [1].

State estimation is a fundamental tool for the situational awareness of ADNs. By processing a redundant set of real-time measurements, along with information from other sources such as virtual measurements and pseudo-measurements, the operating state of the system can be reliably estimated. It is important to improve the accuracy and scope of state estimation for enabling advanced operation and control functions in ADNs.

Existing research on state estimation for distribution networks can be broadly divided into four categories: ① the consideration of different network models such as linear models, three-phase unbalanced models, and decomposed feeder models [2]-[4]; ② the development of more efficient and accurate state estimation algorithms [5]-[7]; ③ the incorporation of new types of measurements such as the advanced metering infrastructure (AMI) and phasor measurement units (PMUs) [8]-[11]; ④ the modeling of pseudo-measurements based on historical data or forecasting techniques aimed to improve the observability and measurement redundancy [12], [13].

In ADNs, a major challenge is the intermittent and stochastic generation nature of DGs, which leads to frequent fluctuation of power flow profiles, power quality issues, and reduced system stability. Battery energy storage systems (BESSs) are one of the most promising solutions to this challenge, which are being rapidly populated in power systems around the world [14]. The state of charge (SOC) is the essential variable to characterize the operating state of batteries, which is defined as the ratio of the remaining capacity of batteries to the total capacity [15]. The SOC is a crucial variable at both the battery level and the power grid level: ① at the BESS level, the SOC is the most important information for evaluating the status of batteries and allowing their output to be controlled smoothly and in balance [16]; ② at the ADN level, the generation dispatch and security assessment applications need to take SOC into consideration. With accurate SOC estimates, the BESS can be operated to provide frequency regulation and load shifting capabilities, among many other functions [17]. However, the SOC cannot be measured directly, and must be estimated based on measurable quantities such as voltage and current. At present, SOC estimation methods can be classified into five branches: ① traditional methods such as Coulomb counting [18]; ② adaptive filtering methods such as extended Kalman filters [19], unscented Kalman filters [20], and $H\infty$ filters [21]; ③ nonlinear observers [22]; ④ machine learning methods

such as neural networks [23], [24] and support vector machines [25]; ⑤ composite estimation methods combining two or more different estimation methods [26]. Based on SOC estimation, a number of applications in battery management have also been explored, e.g., the charging pattern optimization for charging speed [27], balancing of battery cells [28], and electricity bill savings [29]. Due to a number of challenges that have not been fully resolved such as modeling error, measurement error, computational efficiency, and online operation requirements, the SOC estimation is still a very active research area to date.

In the existing literature, the SOC estimation problem has been restricted to the BESS itself, as seen behind the point of common coupling (PCC), disregarding possible synergies and integration with the ADN state estimation. In fact, it is beneficial to bridge this gap for both ADNs and BESSs. For the ADN, grid-scale BESSs are important components to be modeled, and accurate SOC estimation of grid-scale BESSs is an important part of situational awareness required for system dispatch and control [30], [31]. For the BESSs, the joint estimation with the power grid leads to improvement of measurement redundancy, which enhances the capabilities of SOC estimation in the presence of measurement noise, unintentional bad data, and malicious cyber attacks. Unfortunately, studies on the state estimation of ADNs and the SOC estimation of BESSs have so far been conducted by two separate technical communities. No existing work has exploited the linkage between the two estimation problems and developed a holistic estimation framework that benefits both ADNs and BESSs.

This paper is dedicated to bridging the gap between the state estimation of ADNs and the SOC estimation of grid-scale BESSs. It starts by developing models of BESS components that are suitable for state estimation. A holistic estimation framework for ADNs and BESSs is then proposed, with state variables clearly defined and state transition and measurement equations explicitly derived. The largest normalized residual (LNR) test is also applied for the identification and correction of bad data [32]. Compared with existing literature, the main contributions of this paper are summarized as follows.

1) The operating states of ADNs and grid-scale BESSs are estimated under a holistic framework. The partial equivalence between the weighted least squares (WLS) estimator and iterated extended Kalman filter (IEKF) is exploited to fuse the dynamic estimation problem of BESSs characterized by differential equations with the static estimation problem of ADNs characterized by algebraic equations.

2) For ADNs, the situational awareness of power grids is enhanced by extending the monitoring scope of state estimation from power grids to BESSs; in addition, the BESS model and measurements help improve the state estimation accuracy of the grid.

3) For BESSs, the information from the measurements of both BESSs and ADNs is fully exploited, and the increased measurement redundancy enhances the accuracy of SOC estimation and the robustness against bad data.

It will be demonstrated by simulation cases that breaking down the barrier between the two domains brings about significant benefits for both sides.

The rest of the paper is organized as follows. Section II reviews the equivalent circuit models of batteries. Section III presents Kalman filter in a WLS form. The proposed state estimation framework, including the detailed state transition equations, measurement equations, and the WLS-form IEKF, is presented in Section IV. Section V demonstrates the effectiveness of the proposed framework with simulation results. Concluding remarks are given in Section VI.

II. BATTERY EQUIVALENT CIRCUIT MODELS

Lithium-ion batteries with lithium-iron phosphate as cathode material are commonly used in BESSs. An actual battery bank can be represented by an equivalent battery. In turn, an accurate battery model can be used to characterize the external behavior of the battery such as current and voltage, as well as internal characteristics such as electromotive force, internal resistance, and SOC [33]-[35]. The equivalent circuit models that are commonly used include the Rint model, the PNGV model, and the Thevenin equivalent circuit model [36], [37]. With good representation of the electrochemical polarization characteristics and concentration polarization characteristics of a BESS, the second-order Thevenin equivalent circuit model is widely used, as shown in Fig. 1. The two RC networks are used to model the two dynamic processes of internal reactions mentioned above.
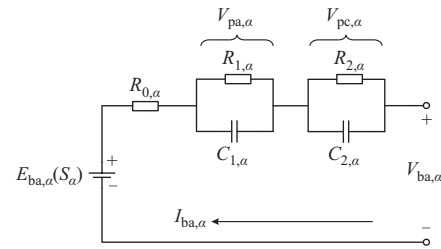

Fig. 1. Second-order Thevenin equivalent model.

In Fig. 1, the subscript α identifies the state variables and measurements associated with a BESS labeled as α; $V_{\mathrm{pa},\alpha}$ and $V_{\mathrm{pc},\alpha}$ are the electrochemical polarization voltage and the concentration polarization voltage of the equivalent model, respectively; S_α is the SOC of the battery; $E_{\mathrm{ba},\alpha}$ is the internal electromotive force of the battery, which is a function of S_α; $R_{1,\alpha}$ and $C_{1,\alpha}$ are the electrochemical polarization resistance and capacitance, respectively; $R_{2,\alpha}$ and $C_{2,\alpha}$ are the concentration polarization resistance and capacitance, respectively; $R_{0,\alpha}$ is the ohmic internal resistance of the battery; $I_{\mathrm{ba},\alpha}$ is the output current of the battery; and $V_{\mathrm{ba},\alpha}$ is the output voltage of the battery. The associated differential equations can be derived as:

$$\begin{cases} \dfrac{\mathrm{d}V_{\mathrm{pa},\alpha}}{\mathrm{d}t} = \dfrac{1}{C_{1,\alpha}}\dfrac{V_{\mathrm{pa},\alpha}}{R_{1,\alpha}} - \dfrac{1}{C_{1,\alpha}}I_{\mathrm{ba},\alpha} \\[2mm] \dfrac{\mathrm{d}V_{\mathrm{pc},\alpha}}{\mathrm{d}t} = \dfrac{1}{C_{2,\alpha}}\dfrac{V_{\mathrm{pc},\alpha}}{R_{2,\alpha}} - \dfrac{1}{C_{2,\alpha}}I_{\mathrm{ba},\alpha} \\[2mm] S_\alpha = S_{0,\alpha} - \dfrac{\eta_\alpha}{C_{n,\alpha}}\displaystyle\int_0^t I_{\mathrm{ba},\alpha}\,\mathrm{d}t \\[2mm] V_{\mathrm{ba},\alpha} = E_{\mathrm{ba},\alpha} - V_{\mathrm{pa},\alpha} - V_{\mathrm{pc},\alpha} - R_{0,\alpha}I_{\mathrm{ba},\alpha} \end{cases} \tag{1}$$

where $S_{0,a}$ is the initial value of SOC; $C_{n,a}$ is the rated capacity of the battery; and η_a is the charging and discharging efficiency of the battery. The unknown parameters in the equivalent model of the battery, i.e., $R_{0,a}$, $R_{1,a}$, $R_{2,a}$, $C_{1,a}$, and $C_{2,a}$, can be identified online by the recursive least square (RLS) method [36]. The variations of the parameters are in a different time scale compared with $V_{pa,a}$, $V_{pc,a}$, and S_a. Thus, they can be considered approximately constant in relatively short operation windows.

III. WLS-FORM IEKF

Most applications in ADN operation are based on the steady-state analysis of the power grid. Therefore, the vast majority of ADN state estimation methods are static methods such as the WLS method, which do not account for state transitions between time instants [2]-[6], [8]-[13]. However, for a BESS, since the SOC and the capacitor voltages are by nature the integral of current over time, a dynamic estimation method such as the IEKF method should be applied. In the holistic estimation problem for an ADN with integrated BESSs, the original forms of either the WLS method or the IEKF method will not be directly applicable. This section will briefly introduce the IEKF method used for dynamic state estimation, and the WLS method used for static state estimation. Then, it will be shown that the correction stage of the IEKF method is equivalent to a WLS estimation problem. This will pave the way for constructing a WLS-form IEKF method for estimating both the static and dynamic state variables in an ADN with BESSs.

A. IEKF Algorithm

For nonlinear dynamic systems described by differential equations, the IEKF is a commonly used algorithm for estimating state evolution. For each time step, it consists of a prediction stage and a correction stage. In the prediction stage, the state estimate in the previous time step is advanced through a predefined process model to find the "a priori state" estimate of the current time step. In the correction stage, the "a priori" state estimate is corrected by the actually collected measurements from the current time step. The time-discretized state transition and measurement equations of a nonlinear dynamic system are given by:

$$x_t = f(x_{t-1}, u_{t-1}) + w_{t-1} \tag{2}$$

$$z_t = h(x_t) + v_t \tag{3}$$

where the subscripts t and $t-1$ represent the variables at the current time step and the previous time step, respectively; x is the state vector; u is the input vector; w is the process noise vector; z is the measurement vector; v is the measurement noise vector; and f and h are the state transition function and the measurement function, respectively.

The prediction stage in the IEKF is used to obtain the "a priori" estimate, denoted by the subscript "(−)", from the "a posteriori" estimate, denoted by the subscript "(+)", from the last time step:

$$\hat{x}_{t(-)} = f(\hat{x}_{t-1(+)}, u_{t-1}) \tag{4}$$

$$P_{t(-)} = F_t P_{t-1} F_t^{\mathrm{T}} + Q_t \tag{5}$$

where the superscript $\hat{\ }$ represents the estimate of a variable; $F = \partial f / \partial x$; P is the covariance matrix of the state estimate; and Q is the covariance matrix of the process noise.

When real-time measurements are actually captured, the correction stage of IEKF determines the "a posteriori" state estimate:

$$K_t = P_{t(-)} H_t^{\mathrm{T}} (H_t P_{t(-)} H_t^{\mathrm{T}} + R_t)^{-1} \tag{6}$$

$$\hat{x}_{t(+)} = \hat{x}_{t(-)} + K_t (z_t - H_t \hat{x}_{t(-)}) \tag{7}$$

$$P_{t(+)} = (I - K_t H_t) P_{t(-)} \tag{8}$$

where I is the identity matrix; $H = \partial h / \partial x$; R is the covariance matrix of the measurement noise; and K is the well-known Kalman gain. It should be noted that in IEKF, the correction stage equations should be performed iteratively. After executing (6) and (7) once, one should set $\hat{x}_{t(-)}$ as $\hat{x}_{t(+)}$, update H_t, and execute (6) and (7) over again until $\hat{x}_{t(+)}$ converges to a stable value.

B. WLS Algorithm

In the widely studied state estimation problem of the power grid, network equations are algebraic in the phasor domain. The WLS model, which minimizes the weighted sum of the measurement residuals at the current time step, is adopted. At time step t, the WLS formulation can be presented as:

$$\hat{x}_t = \underset{x_t}{\arg\min}\ (z_t - h(x_t))^{\mathrm{T}} R_t^{-1} (z_t - h(x_t)) \tag{9}$$

The covariance matrix of the state estimate is given by:

$$P_{t(+)} = (H_t^{\mathrm{T}} R_t^{-1} H_t)^{-1} \triangleq G_t^{-1} \tag{10}$$

In this estimation model, the estimates of state variables x_t are determined by the measurements at the current time step z_t only.

C. WLS-form IEKF Algorithm

Although the formulations of IFKF and WLS seem to be very different, there is an inherent connection between the two. In fact, it can be shown that the correction stage of IEKF, written as (6)-(8), can be converted to solving an equivalent WLS problem [37]:

$$\begin{aligned}
\hat{x}_{t(+)} = \ &\underset{x_t}{\arg\min}\ \Big\{ (z_t - h_t(x_t))^{\mathrm{T}} R_t^{-1} (z_t - h_t(x_t)) + \\
&(\hat{x}_{t(-)} - x_t)^{\mathrm{T}} P_{t(-)}^{-1} (\hat{x}_{t(-)} - x_t) \Big\} = \\
&\underset{x_t}{\arg\min}\ \Big\{ (\tilde{z}_t - \tilde{h}_t(x_t))^{\mathrm{T}} \tilde{R}_t^{-1} (\tilde{z}_t - \tilde{h}_t(x_t)) \Big\}
\end{aligned} \tag{11}$$

where $\tilde{z}_t = (z_t^{\mathrm{T}}, \hat{x}_{t(-)}^{\mathrm{T}})^{\mathrm{T}}$; $\tilde{R}_t = \mathrm{diag}(R_t, P_{t(-)})$; $\tilde{H}_t^{\mathrm{T}} = \partial \tilde{h}_t / \partial x_t$; and $\tilde{h}_t(x_t) = (\tilde{h}_t(x_t)^{\mathrm{T}}, x_t^{\mathrm{T}})^{\mathrm{T}}$. The covariance matrix of the state estimate is given by:

$$P_{t(+)} = (\tilde{H}_t^{\mathrm{T}} \tilde{R}_t^{-1} \tilde{H}_t)^{-1} \triangleq \tilde{G}_t^{-1} \tag{12}$$

It is already proven that (7) and (8) are equivalent to (11) and (12), respectively. In other words, the correction stage of IEKF is equivalent to performing a WLS-based "static state estimation", with the measurement vector including the actual measurements from the current time step z_t, and the "a priori" state estimate $\hat{x}_{t(-)}$ obtained from the prediction stage as pseudo-measurements. This equivalence property will be exploited in the development of a framework for estimating

the state variables of an ADN with integrated BESSs.

IV. STATE ESTIMATION OF ADN WITH BESSs

This section develops a state estimation framework for an ADN with BESSs. The state variables that can characterize the operating state of the system will be selected, and state transition equations and measurement equations associated with available sensors in the BESS will be derived. A WLS-form IEKF method and the LNR method will be presented for state estimation and bad data processing, respectively. Before moving forward, there are two points to be made clear.

1) In literature, a large volume of research has been dedicated to addressing specific issues pertaining to ADN state estimation. For example, solutions to the unbalanced three phases can be found in [2], [3]; solutions to the integration of diverse types of sensor measurements (supervisory control and data acquisition (SCADA), PMU, AMI, etc.) can be found in [8]-[11]; and solutions to the lack of observability or measurement redundancy can be found in [12], [13]. Obviously, these issues do not automatically disappear when it comes to the state estimation of an ADN with BESSs. However, as they have already been extensively investigated in numerous publications, it is neither possible nor necessary to reiterate all of them in this single paper. Thus, this paper is dedicated to presenting the fusion of ADN state estimation and BESS SOC estimation into one holistic paradigm, which constitutes the core innovation of the paper. Due to its generality, the proposed work can be readily combined with solutions presented in [2], [3], [8]-[13] to address the aforementioned issues in ADN state estimation as needed.

2) While the discussion focuses on distribution systems where BESSs are proliferating rapidly, the proposed estimation framework is general enough to be used for the monitoring of BESSs in transmission systems, since both the transmission system state estimation and the distribution system state estimation share the same core engine (WLS estimator based on steady-state algebraic network equations). As is evident, massive-scale BESSs have been and will continue to be deployed in transmission systems as well [38].

A. State Transition Equations and Measurement Equations

The structure of a grid-connected BESS is illustrated in Fig. 2. The main components include the battery array, the DC/DC converter, the DC/AC inverter, and the transformer.
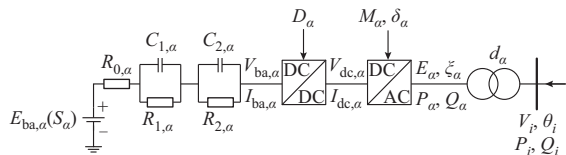

Fig. 2.   Structure of grid-connected BESS.

Suppose the PCC of the BESS (labeled as α) is bus i of the power grid; V_i and θ_i are the voltage magnitude and phase angle of the PCC, respectively; P_i and Q_i are the active and reactive power injected into the PCC, respectively; d_α is the transformer ratio; M_α and δ_α are the modulation ratio and the modulation phase angle of the DC/AC converter,

respectively; E_α and ξ_α are the output voltage magnitude and the voltage phase angle of the DC/AC converter, respectively; $V_{dc,\alpha}$ and $I_{dc,\alpha}$ are the output voltage and current of the DC/DC converter, respectively; and D_α is the duty ratio of the DC/DC converter. In the state transition equations and measurement equations derived below, superscripts w, v, and z denote the process noise, measurement noise, and measured values, respectively. In the measurement equations, the time step notation (t) is dropped.

In the equivalent model of the battery, S_α, $V_{pa,\alpha}$, and $V_{pc,\alpha}$ are selected as state variables. Equation (1) is discretized with time interval T into the state transition equations:

$$V_{pa,\alpha}(t) = e^{-T/(R_{1,\alpha}C_{1,\alpha})}V_{pa,\alpha}(t-1) +$$
$$R_{1,\alpha}(1 - e^{-T/(R_{1,\alpha}C_{1,\alpha})})I_{ba,\alpha}(t-1) + V_{pa,\alpha}^w(t-1) \quad (13)$$

$$V_{pc,\alpha}(t) = e^{-T/(R_{2,\alpha}C_{2,\alpha})}V_{pc,\alpha}(t-1) +$$
$$R_{2,\alpha}(1 - e^{-T/(R_{2,\alpha}C_{2,\alpha})})I_{ba,\alpha}(t-1) + V_{pc,\alpha}^w(t-1) \quad (14)$$

$$S_\alpha(t) = S_\alpha(t-1) + \frac{\eta_\alpha T}{C_{n,\alpha}}I_{ba,\alpha}(t-1) + S_\alpha^w(t-1) \quad (15)$$

At the same time, $V_{ba,\alpha}$ and $I_{ba,\alpha}$ are the measurable variables, and their measurement equations can be expressed as:

$$I_{ba,\alpha}^z = I_{ba,\alpha} + I_{ba,\alpha}^v \quad (16)$$

$$V_{ba,\alpha}^z = E_{ba,\alpha}(S_\alpha) - V_{pa,\alpha} - V_{pc,\alpha} - R_{0,\alpha}I_{ba,\alpha} + V_{ba,\alpha}^v \quad (17)$$

Next, the state transition equations and measurement equations for the power converters will be considered. The dynamics of power converters are in the time scale of microseconds, which are several orders smaller in magnitude than the time scale of the battery dynamics. Hence, the power converters can be treated as being in steady state, described by algebraic equations. Therefore, state transition equations do not apply, and only measurement equations need to be derived.

Denote the efficiency of the DC/DC converter as $\eta_{dc/dc,\alpha}$, and select $V_{dc,\alpha}$ and $I_{ba,\alpha}$ as state variables. The measurement equations can be derived as:

$$D_\alpha^z = 1 - \frac{V_{dc,\alpha}}{E_{ba,\alpha}(S_\alpha) - V_{pa,\alpha} - V_{pc,\alpha} - R_{0,\alpha}I_{ba,\alpha}} + D_\alpha^v \quad (18)$$

$$V_{dc,\alpha}^z = V_{dc,\alpha} + V_{dc,\alpha}^v \quad (19)$$

$$I_{dc,\alpha}^z = \eta_{dc/dc,\alpha}\frac{I_{ba,\alpha}}{V_{dc,\alpha}}(E_{ba,\alpha}(S_\alpha) - V_{pa,\alpha} - V_{pc,\alpha} - R_{0,\alpha}I_{ba,\alpha}) + I_{dc,\alpha}^v \quad (20)$$

Denote the efficiency of the DC/AC converter as $\eta_{dc/ac,\alpha}$, and select the output voltage magnitude E_α and phase angle δ_α as state variables. The measurement equations are expressed as:

$$M_\alpha^z = \frac{E_\alpha}{V_{dc,\alpha}} + M_\alpha^v \quad (21)$$

$$E_\alpha^z = E_\alpha + E_\alpha^v \quad (22)$$

$$\delta_\alpha^z = \theta_i - \xi_\alpha + \delta_\alpha^v \quad (23)$$

As mentioned at the beginning of this subsection, it is assumed that the PCC of the BESS is bus i of the ADN. Hence, V_i and θ_i can be selected as state variables, and the measurement equations can be expressed as:

$$V_i^z = V_i + V_i^v \tag{24}$$

$$P_\alpha^z = E_\alpha(g_{s\alpha} + g_{\alpha i}) - E_\alpha V_i(g_{\alpha i}\cos(\xi_\alpha - \theta_i) + b_{\alpha i}\sin(\xi_\alpha - \theta_i)) + P_\alpha^v \tag{25}$$

$$Q_\alpha^z = -E_\alpha(b_{s\alpha} + b_{\alpha i}) - E_\alpha V_i(g_{\alpha i}\cos(\xi_\alpha - \theta_i) - b_{\alpha i}\sin(\xi_\alpha - \theta_i)) + Q_\alpha^v \tag{26}$$

$$P_i^z = h_{pi}(V_i, V_j, \ldots, \theta_i, \theta_j, \ldots) - E_\alpha(g_{s\alpha} + g_{\alpha i}) + E_\alpha V_i(g_{\alpha i}\cos(\xi_\alpha - \theta_i) + b_{\alpha i}\sin(\xi_\alpha - \theta_i)) + P_i^v \tag{27}$$

$$Q_i^z = h_{qi}(V_i, V_j, \ldots, \theta_i, \theta_j, \ldots) + E_\alpha(b_{s\alpha} + b_{\alpha i}) + E_\alpha V_i(g_{\alpha i}\cos(\xi_\alpha - \theta_i) - b_{\alpha i}\sin(\xi_\alpha - \theta_i)) + Q_i^v \tag{28}$$

$$0 = \eta_{dc/dc,\alpha}\eta_{dc/ac,\alpha}I_{ba,\alpha}(E_{ba,\alpha}(S_\alpha) - V_{pa,\alpha} - V_{pc,\alpha} - R_{0,\alpha}I_{ba,\alpha}) - E_\alpha^2(g_{s\alpha} + g_{\alpha i}) + E_\alpha V_i(g_{\alpha i}\cos(\xi_\alpha - \theta_i) + b_{\alpha i}\sin(\xi_\alpha - \theta_i)) + \Delta P_\alpha^z \tag{29}$$

where $h_{pi}(\cdot)$ and $h_{qi}(\cdot)$ describe the relationships between the voltage magnitudes and phase angles of the buses in the ADN and the injected active and reactive power at bus i, respectively; and $g_{s\alpha} + jb_{s\alpha}$ and $g_{\alpha i} + jb_{\alpha i}$ are the shunt and series admittances derived from the transformer model, respectively. Equation (29) is a virtual measurement describing the power conservation law.

In summary, in order to monitor the state of BESS α, the dynamic state variables, i.e., state variables associated with differential equations, in BESS α are defined as:

$$x_{d,\alpha} = [S_\alpha, V_{pa,\alpha}, V_{pc,\alpha}]^T \tag{30}$$

The static state variables, i.e., state variables associated with algebraic equations only, are defined as:

$$x_{s,\alpha} = [I_{ba,\alpha}, V_{dc,\alpha}, E_\alpha, \delta_\alpha]^T \tag{31}$$

The overall state vector is defined as:

$$x_\alpha = [S_\alpha, V_{pa,\alpha}, V_{pc,\alpha}, I_{ba,\alpha}, V_{dc,\alpha}, E_\alpha, \delta_\alpha]^T \tag{32}$$

Note that V_i and θ_i are left out of the list since they are state variables of the ADN.

The collective measurement vector is defined as:

$$z_\alpha = [V_{ba,\alpha}^z, I_{ba,\alpha}^z, D_\alpha^z, V_{dc,\alpha}^z, I_{dc,\alpha}^z, M_\alpha^z, E_\alpha^z, \delta_\alpha^z, P_\alpha^z, Q_\alpha^z, 0]^T \tag{33}$$

Note that V_i^z, P_i^z, and Q_i^z are left out of the list since they are measurements of the ADN.

For ADNs, the state variables are the voltage magnitude V_i and phase angle θ_i. The measurements mainly include the voltage magnitude V_i, the active and reactive power injections of each bus P_i and Q_i, and the active and reactive power flows of each branch P_{ij} and Q_{ij}. Detailed measurement equations in the power grid can be found in [39].

The state variables in the power grid are:

$$x_N = [V_1, V_2, \ldots, V_i, \ldots, \theta_1, \theta_2, \ldots, \theta_i, \ldots]^T \tag{34}$$

The measurements in the power grid are:

$$z_N = [V_1, V_2, \ldots, V_i, \ldots, P_1, P_2, \ldots, P_i, \ldots, Q_1, Q_2, \ldots, Q_i, \ldots, P_{ij}, \ldots, Q_{ij}, \ldots]^T \tag{35}$$

B. Joint State Estimation for BESSs and ADNs

For an ADN with multiple BESSs ($\alpha, \beta, \ldots, \zeta$), one has:

$$z = [z_\alpha, z_\beta, \ldots, z_\zeta, z_N]^T \tag{36}$$

$$x = [x_\alpha, x_\beta, \ldots, x_\zeta, x_N]^T \tag{37}$$

where z and x are the collective measurement vector and the state vector of the whole system, respectively.

From the last subsection, recall that for the BESS, some of the state variables are dynamic, while others are static. In the ADN, all the state variables are static. In this paper, a WLS-form IEKF estimator will be developed to jointly estimate the dynamic and static state variables of the whole system. The state vector can be reorganized by separating the dynamic and static state variables:

$$x = [x_{d,\alpha}^T, x_{s,\alpha}^T, x_{d,\beta}^T, x_{s,\beta}^T, \ldots, x_{d,\zeta}^T, x_{s,\zeta}^T, x_N^T]^T = [x_{d,\alpha}^T, x_{d,\beta}^T, \ldots, x_{d,\zeta}^T, x_{s,\alpha}^T, x_{s,\zeta}^T, \ldots, x_{s,\beta}^T, x_N^T]^T = [x_d^T, x_s^T]^T \tag{38}$$

The procedure for estimating the state of an ADN with BESSs are summarized as follows.

Step 1: set time step $t = 0$. Initialize the "a posteriori" estimate of state variables $\hat{x}_{t(+)} = [\hat{x}_{d,t(+)}^T, \hat{x}_{s,t(+)}^T]^T$, and the covariance matrix of the "a posteriori" estimate of dynamic state variables $P_{d,t(+)}$. Set the state estimate tolerance $\tau > 0$, bad data detection threshold $c > 0$, and time window T for executing state estimation.

Step 2: set $t \leftarrow t + 1$.

Step 3: prediction stage. Based on the state transition equations, predict the "a priori" estimate of the dynamic state variables $\hat{x}_{d,t(-)}$ at time t as (39).

$$\hat{x}_{d,t(-)} = f(\hat{x}_{d,t-1(+)}, u_{d,t-1(+)}) \tag{39}$$

where f is derived from (14)-(16). Note that these state transition equations are actually linear. Therefore, the "a priori" estimate of the dynamic state variables $\hat{x}_{d,t(-)}$ is an unbiased estimate if the process noise has zero mean.

Step 4: evaluate the covariance matrix:

$$P_{d,t(-)} = F_{t-1}^T P_{d,t-1(+)} F_{t-1} + Q_{d,t-1} \tag{40}$$

Step 5: correction stage. Solve the following WLS problem:

$$\{\hat{x}_{d,t(+)}, \hat{x}_{s,t(+)}\} = \underset{\{x_{d,t}, x_{s,t}\}}{\arg\min}\ \{(z_t - h_t(x_{d,t}, x_{s,t}))^T R_t^{-1} \cdot$$
$$(z_t - h_t(x_{d,t}, x_{s,t})) + (\hat{x}_{d,t(-)} - x_{d,t})^T P_{d,t(-)}^{-1}(\hat{x}_{d,t(-)} - x_{d,t})\} =$$
$$\underset{x_t}{\arg\min}\ \{(\tilde{z}_t - \tilde{h}_t(x_t))^T \tilde{R}_t^{-1}(\tilde{z}_t - \tilde{h}_t(x_t))\} \tag{41}$$

where $\tilde{z}_t = [z_t^T, \hat{x}_{d,t(-)}^T]^T$; $\tilde{h}_t(x_t) = [(\tilde{h}_t(x_t))^T, x_{d,t}^T]^T$; and $\tilde{R}_t = \text{diag}(R_t, P_{d,t(-)})$. The Gauss-Newton method can be used for solving this problem, detailed as follows.

1) Set iteration number $k = 0$. Initialize state variables $x_{k,t} = [x_{d,k,t}^T, x_{s,k,t}^T]^T$.

2) Evaluate the Jacobian matrix and the gain matrix as:

$$\tilde{H}_{k,t}(x_{k,t}) = \frac{\partial \tilde{h}_{k,t}(x_{k,t})}{\partial x_{k,t}} \tag{42}$$

$$\tilde{G}_{k,t}(x_{k,t}) = \tilde{H}_{k,t}^T(x_{k,t})\tilde{R}_{k,t}^{-1}\tilde{H}_{k,t}(x_{k,t}) \tag{43}$$

3) Evaluate the state update vector as:

$$\Delta x_{k,t} = (\tilde{G}_{k,t}(x_{k,t}))^{-1}\tilde{H}_{k,t}^T(x_{k,t})R_{k,t}^{-1}(\tilde{z}_{k,t} - \tilde{h}_{k,t}(x_{k,t})) \tag{44}$$

4) Update the state estimate vector by:

$$x_{k+1,t} = x_{k,t} + \Delta x_{k,t} \tag{45}$$

5) If $\|\Delta x_{k,t}\|_\infty > \tau$, set $k \leftarrow k+1$, and return to 2); otherwise, set $\hat{x}_{t(+)} = x_{k,t}$ and $\tilde{H}_t = \tilde{H}_{k,t}$, and proceed to Step 6. The "a pos-

teriori" estimate of all state variables $\hat{\boldsymbol{x}}_{t(+)}$ is an unbiased estimate if the measurement error has zero mean.

Step 6: evaluate the covariance matrix of the state estimate as:

$$\boldsymbol{P}_{t(+)} = (\tilde{\boldsymbol{H}}_t^{\mathrm{T}} \tilde{\boldsymbol{R}}_t^{-1} \tilde{\boldsymbol{H}}_t)^{-1} \triangleq \tilde{\boldsymbol{G}}_t^{-1} \tag{46}$$

The covariance matrix of the "a posteriori" estimate of dynamic state variables, which is needed to perform prediction in the next time step, can be obtained by extracting the diagonal block of $\boldsymbol{P}_{t(+)}$ corresponding to the dynamic state variables $\boldsymbol{P}_{\mathrm{d}, t(+)}$.

Step 7: identify and correct bad data by performing the LNR test.

1) The value of the normalized residual is obtained by:

$$\tilde{\boldsymbol{r}}_t^{\mathrm{N}} = (\mathrm{diag}(\tilde{\boldsymbol{\Omega}}_t))^{-\frac{1}{2}} \tilde{\boldsymbol{r}}_t \tag{47}$$

where $\tilde{\boldsymbol{\Omega}}_t = \tilde{\boldsymbol{R}}_t - \tilde{\boldsymbol{H}}_t(\hat{\boldsymbol{x}}_{t(+)})(\tilde{\boldsymbol{H}}_t^{\mathrm{T}}(\hat{\boldsymbol{x}}_{t(+)})\tilde{\boldsymbol{R}}_t^{-1}\tilde{\boldsymbol{H}}_t(\hat{\boldsymbol{x}}_{t(+)}))^{-1}\tilde{\boldsymbol{H}}_t^{\mathrm{T}}(\hat{\boldsymbol{x}}_{t(+)})$ is the residual covariance matrix; and $\tilde{\boldsymbol{r}}_t = \tilde{\boldsymbol{z}}_t - \tilde{\boldsymbol{h}}_t(\hat{\boldsymbol{x}}_{t(+)})$ is the residual vector.

2) Find the measurement corresponding to the LNR as:

$$u = \arg\min_{j} \{\tilde{r}_{t,j}^{\mathrm{N}}\} \tag{48}$$

where $\tilde{r}_{t,j}^{\mathrm{N}}$ is the jth entry of vector $\tilde{\boldsymbol{r}}_t^{\mathrm{N}}$.

3) If $|\tilde{r}_{t,u}^{\mathrm{N}}| > c$, correct the corresponding measurement by (49) and return to *Step 5*. Otherwise, process to *Step 8*.

$$\tilde{z}_{t,u} \leftarrow \tilde{z}_{t,u} - \frac{\tilde{R}_{t,uu}}{\tilde{\Omega}_{t,uu}} \tilde{r}_{t,u} \tag{49}$$

where $\tilde{z}_{t,u}$, $\tilde{R}_{t,uu}$, $\tilde{\Omega}_{t,uu}$, and $\tilde{r}_{t,u}$ are the elements of $\tilde{\boldsymbol{z}}_t$, $\tilde{\boldsymbol{R}}_t$, $\tilde{\boldsymbol{\Omega}}_t$, and $\tilde{\boldsymbol{r}}_t$, respectively.

Step 8: return to *Step 2* if $t < T$; otherwise, terminate the procedure.

In reality, the covariance matrices for process noise and measurement noise $\boldsymbol{Q}_t$ and $\boldsymbol{R}_t$ can be assigned based on the confidence on battery models and the accuracy classes of sensors. If they are difficult to determine, adaptive estimation methods can be applied to obtain optimal values of $\boldsymbol{Q}_t$ and $\boldsymbol{R}_t$ that yield high estimation accuracy [40], [41]. It should also be noted that the uncertainty resulting from long-term phenomenon such as capacity decreases due to aging, existing capacity prediction works can be applied in parallel to the proposed work to form a complete monitoring solution over the battery life [42]-[44].

Remark 1: in this procedure, only the dynamic state variables are involved in the prediction stage, i.e., *Step 3*, and both the dynamic and static state variables are involved in the correction stage, i.e., *Step 5*.

Remark 2: in the correction stage, the "a priori" estimates of the dynamic states acts as if they are additional pseudo-measurements, providing extra information in addition to the actually collected real-time measurements.

Remark 3: in the WLS-form correction stage, the inverse of the gain matrix $\tilde{\boldsymbol{G}}_t^{-1}$ is the covariance matrix of the state estimate. Therefore, it can be used to extract the covariance of the "a posteriori" estimate of the dynamic state variables.

Remark 4: thanks to the correction stage, the LNR test can be performed to detect and identify the bad data.

V. CASE STUDY

In order to verify the effectiveness of the proposed framework, the IEEE 33-bus test system is used for simulation. The system topology and measurement configuration are shown in Fig. 3, where "N" denotes the real and reactive power injections and "PF" denotes the real and reactive branch flows. In addition, the voltages at buses 1, 2, 4, 15, 21 are also measured. Two BESSs, denoted as α and β, are connected to buses 14 and 26, respectively. While a distribution system is chosen for case study, it should be noted that the general WLS-form IEKF estimation framework is applicable to transmission systems as well. The maximum power output and energy storage capacity are 0.18 MW and 800 Ah, respectively. A nine-order polynomial is used to represent the relation between the SOC and the internal electromotive force, $E_{\mathrm{ba}}(S)$. Both the BESSs operate in the discharging mode with an initial SOC of 0.7. The efficiencies of the DC/DC converter and DC/AC converter are 95% and 96%, respectively. The discharging current is 400 A, and the discharging voltage is 450 V. The output voltage magnitude of the DC/DC converter is 600 V, and the input voltage magnitude of the DC/AC converter is 99.44 V.
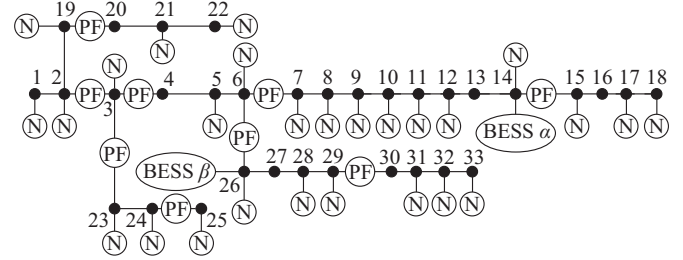

Fig. 3.   IEEE 33-bus test system with BESSs.

A. State Estimation in Presence of Random Noise

In order to compare the accuracy of the proposed holistic estimation framework with the conventional siloed frameworks of BESS SOC estimation and ADN state estimation, the process noise and measurement noise obeying Gaussian distributions are introduced. The process noise may come from inaccurate modeling or small disturbances that the model cannot account for in reality, and its magnitude is typically much lower than that of measurement noise. Results are averaged over 20 executions and 1500 s in each simulation case.

1) Improvement for BESS SOC Estimation

For the BESS, the comparison between the root mean square errors (RMSEs) of the SOC estimation results using the proposed holistic estimation framework and the conventional BESS SOC estimation framework [19] under various noise conditions is shown in Table I. In the table, SD stands for standard deviation, and RMSE stands for root mean square error. Note that the simulated noise conditions range from the typical SCADA measurement accuracy level to the typical pseudo-measurement accuracy level in the ADN. Under various conditions, the proposed holistic estimation framework achieves higher accuracy for the SOC estimate than the conventional BESS SOC estimation framework

where the battery model is isolated from the grid model. This improvement meets the expectation since the joint modeling and estimation of the BESS and the power grid improve the measurement redundancy, which leads to better filtering effect of IEKF.

TABLE I
SOC ESTIMATION RESULTS USING PROPOSED HOLISTIC ESTIMATION FRAMEWORK AND CONVENTIONAL ISOLATED BATTERY MODEL

SD of process noise (BESS) (%/s)	SD of measurement noise (P, Q in ADN) (%)	SD of measurement noise (BESS; V in ADN) (%)	RMSE of SOC estimate (isolated)	RMSE of SOC estimate (holistic)
0.005	1	0.1	1.15×10^{-5}	9.09×10^{-6}
0.015	3	0.3	2.28×10^{-5}	1.78×10^{-5}
0.025	5	0.5	4.85×10^{-5}	3.91×10^{-5}
0.035	7	0.7	6.15×10^{-5}	5.90×10^{-5}
0.045	9	0.9	9.34×10^{-5}	8.25×10^{-5}

2) Improvement for ADN State Estimation

For the ADN, simulation results in two different noise scenarios are presented, as specified in Table II.

1) In scenario 1, the measurement noise of the BESS is significantly lower than the measurement noise of the ADN voltages (0.1% versus 0.5%).

2) In scenario 2, the measurement noise of the BESS is significantly higher than that of the ADN voltages (0.9% versus 0.5%).

TABLE II
STANDARD DEVIATIONS OF NOISE IN TWO SCENARIOS

Scenario	SD of process noise (BESS) (%/s)	SD of measurement noise (BESS) (%)	SD of measurement noise (V in ADN) (%)	SD of measurement noise (P, Q in ADN) (%)
1	0.005	0.1	0.5	5
2	0.045	0.9	0.5	5

The MAEs of voltage estimates in these two scenarios are shown in Figs. 4 and 5, respectively. For the two scenarios, the following observations are obtained.
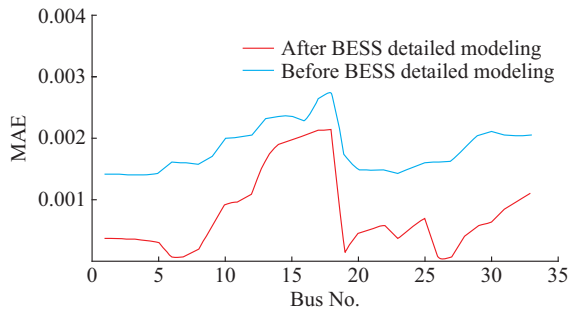

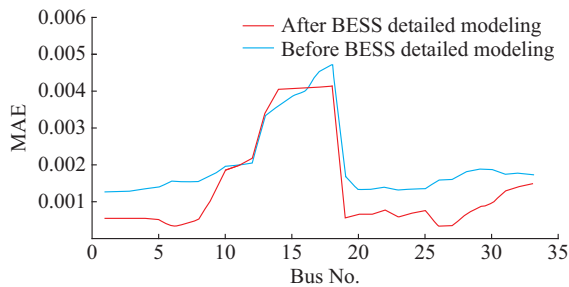Fig. 4.　MAEs of voltage estimates of IEEE 33-bus system in scenario 1.

Fig. 5.　MAEs of voltage estimates of IEEE 33-bus system in scenario 2.

1) For scenario 1, the proposed holistic estimation yields significantly more accurate results compared with the conventional BESS SOC estimation and ADN state estimation.

This is easily understood from the fact that the BESS measurements have higher accuracy than the ADN measurements, and the incorporation of BESS measurements helps improve the accuracy of ADN state estimation.

2) For scenario 2, it is discovered that the proposed holistic estimation also outperforms the conventional BESS SOC estimation and ADN state estimation for a vast majority of buses. This is particularly interesting, since the BESS measurements have lower accuracy than the ADN measurements, and it is not intuitive to understand how the BESS measurements can still enhance the ADN state estimation. The reason is that the BESS SOC estimation contains state transition equations, which fuse information from measurements at different time instants. Since the measurement noise is centered around zero, its effects tend to be smoothed out, yielding a smooth state estimate trajectory with small errors. In contrast, when the BESS SOC estimation is not incorporated, no state transition equations are involved in the ADN state estimation, and the estimation processes for each time instant are completely separate. In that case, no smoothing effect can be achieved.

Based on the results presented above, it can be concluded that the proposed holistic estimation brings mutual benefits for both the accuracy of ADN state estimation and the accuracy of BESS SOC estimation.

B. State Estimation in Presence of Bad Data

In order to verify the bad data processing capability of the proposed holistic estimation, several artificial bad data are introduced, and the LNR-based bad data processing approach

is performed. Specifically, bad data are introduced into the battery output current of BESS α ($I_{ba,\alpha}$), the voltage at bus 21 of the ADN (V_{21}), and the active power injectes into bus 25 of the ADN (P_{25}), respectively. The introduced error magnitudes and time intervals are shown in Table III. In addition to the bad data, the noise of 0.005%/s in state evolution, 1% in power measurements, 0.1% in voltage measurements and BESS SOC measurements, are introduced simultaneously.

TABLE III
INTRODUCED ERRONEOUS VALUES AND TIME INTERVALS

Measurement	True value (p.u.)	Erroneous value (p.u.)	Time interval (s)
$I_{ba,\alpha}$	0.7596	1.5240	400-600
V_{21}	0.9935	1.3388	800-1000
P_{25}	−0.0420	−0.0830	1200-1400

For the BESS, the trajectories of the estimated output currents and SOCs of the BESS α with and without the bad data processing are shown in Figs. 6 and 7, respectively. Between 400 s and 600 s, the measured output current of the battery is erroneous. Without the bad data processing, the output current cannot be effectively estimated, and since the change of the SOC is the integral of the output current, the estimated SOC will deviate from the true value. In contrast, when the bad data processing is preformed, the output current can be corrected and the trajectory of the SOC estimate will remain close to the true trajectory. From the presented results, two observations are particularly noticeable.
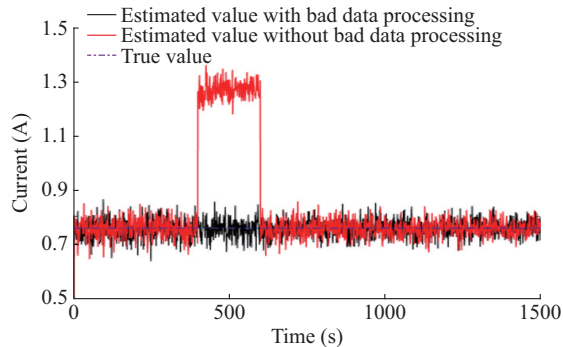

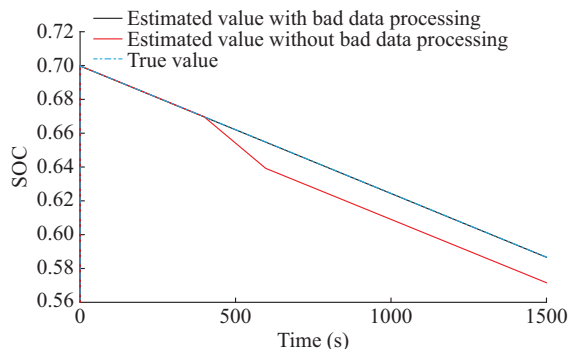Fig. 6.   Estimated battery output currents of BESS α in the presence of bad data.

Fig. 7.   Estimated SOCs of BESS α in the presence of bad data.

1) The battery output/input current is a crucial variable for BESS SOC estimation. Bad data in the output current measurement will result in the deviation of the SOC estimate from the true trajectory, and this impact will persist even after the bad data are cleared for a long time.

2) The bad data identification and correction capability for the output current of a battery is achieved by the proposed holistic state estimation. It provides the measurement redundancy necessary for carrying out the bad data processing. If the BESS SOC estimation is isolated from the ADN state estimation as is conventionally done, it would not be possible to identify and correct errors in the output current, thus the SOC estimate would be left vulnerable.

For the ADN, the estimated voltage at bus 25 is shown in Fig. 8. Without bad data processing, large deviations from the true values can be observed in the results. When the bad data processing is performed, the impacts of the errors in the measurements of both the BESS SOC estimation and ADN state estimation are eliminated, and the estimated values keep track of the true state trajectory effectively.
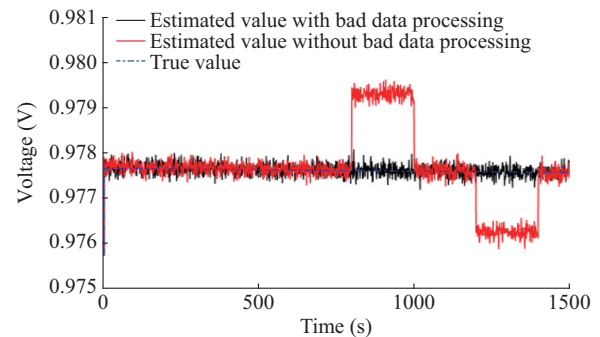

Fig. 8.   Estimated voltage at bus 25 in the presence of bad data.

C. Computational Efficiency

The proposed holistic state estimation is implemented in MATLAB 2018a environment, and tested on a personal computer with a 4-core 2.5 GHz CPU and 16 GB RAM. Over 1500 time steps of the simulation, the average computational time taken by each time step is 0.083 s. For the purposes of ADN and BESS monitoring and control, the required frequency of algorithm execution will be in the time scale of seconds or lower, so the proposed framework can readily satisfy real-time application requirements.

VI. CONCLUSION

In this paper, a holistic framework for the state estimation of ADN with BESSs is proposed. Based on the developed BESS model, the state transition and measurement equations of the grid-connected BESS are derived, and a holistic state estimation and bad data processing formulation is presented for capturing the operating states of both the ADN and BESS.

The simulation results show that the proposed framework achieves significantly higher estimation accuracy compared with performing state estimation for the power grid and SOC estimation for the battery separately. In addition, the proposed framework enables bad data identification and cor-

rection for the BESS SOC estimation. It is found that the gross error in the output current measurement of a BESS has crucial and persistent impact on SOC estimate. By performing bad data identification and correction, the effect of bad data can be effectively eliminated.

The proposed framework is expected to enhance the situational awareness and facilitate the development of reliable and economic ADN operation paradigm with full exploitation of BESS capabilities. In future work, the proposed framework will be further extended to provide a holistic situational awareness solution to integrated and renewable energy systems [45], [46].

REFERENCES

[1] A. K. Marvasti, Y. Fu, S. DorMohammadi *et al.*, "Optimal operation of active distribution grids: a system of systems framework," *IEEE Transactions on Smart Grid*, vol. 5, no. 3, pp. 1228-1237, May 2014.

[2] M. C. de Almeida and L. F. Ochoa, "An improved three-phase AMB distribution system state estimator," *IEEE Transactions on Power Systems*, vol. 32, no. 2, pp. 1463-1473, Mar. 2017.

[3] Y. Liu, J. Li, and L. Wu, "State estimation of three-phase four-conductor distribution systems with real-time data from selective smart meters," *IEEE Transactions on Power Systems*, vol. 34, no. 4, pp. 2632-2643, Jul. 2019.

[4] M. E. Baran and A. W. Kelley, "A branch-current-based state estimation method for distribution systems," *IEEE Transactions on Power Systems*, vol. 10, no. 1, pp. 483-491, Feb. 1995.

[5] C. Gomez-Quiles, A. Gomez-Exposito, and A. de la Villa Jaen, "State estimation for smart distribution substations," *IEEE Transactions on Smart Grid*, vol. 3, no. 2, pp. 986-995, Jun. 2012.

[6] D. A. Haughton and G. T. Heydt, "A linear state estimation formulation for smart distribution systems," *IEEE Transactions on Power Systems*, vol. 28, no. 2, pp. 1187-1195, May 2013.

[7] R. Huang, G. Cokkinides, C. Hedrington *et al.*, "Distribution system distributed quasi-dynamic state estimator," *IEEE Transactions on Smart Grid*, vol. 7, no. 6, pp. 2761-2770, Nov. 2016.

[8] S. Prasad and D. M. V. Kumar, "Trade-offs in PMU and IED deployment for active distribution state estimation using multi-objective evolutionary algorithm," *IEEE Transactions on Instrumentation and Measurement*, vol. 67, no. 6, pp. 1298-1307, Jun. 2018.

[9] P. A. Pegoraro, A. Meloni, L. Atzori *et al.*, "PMU-based distribution system state estimation with adaptive accuracy exploiting local decision metrics and IoT paradigm," *IEEE Transactions on Instrumentation and Measurement*, vol. 66, no. 4, pp. 704-714, Apr. 2017.

[10] A. Alimardani, F. Therrien, D. Atanackovic *et al.*, "Distribution system state estimation based on nonsynchronized smart meters," *IEEE Transactions on Smart Grid*, vol. 6, no. 6, pp. 2919-2928, Nov. 2015.

[11] A. Gómez-Expósito, C. Gómez-Quiles, and I. Džafić, "State estimation in two time scales for smart distribution systems," *IEEE Transactions on Smart Grid*, vol. 6, no. 1, pp. 421-430, Jan. 2015.

[12] A. Angioni, T. Schlösser, F. Ponci *et al.*, "Impact of pseudo-measurements from new power profiles on state estimation in low-voltage grids," *IEEE Transactions on Instrumentation and Measurement*, vol. 65, no. 1, pp. 70-77, Jan. 2016.

[13] Y. Huang, Q. Xu, C. Hu *et al.*, "Probabilistic state estimation approach for AC/MTDC distribution system using deep belief network with non-Gaussian uncertainties," *IEEE Sensors Journal*, vol. 19, no. 20, pp. 9422-9430, Oct. 2019.

[14] M. T. Lawder, B. Suthar, P. W. C. Northrop *et al.*, "Battery energy storage system (BESS) and battery management system (BMS) for grid-scale applications," *Proceedings of the IEEE*, vol. 102, no. 6, pp. 1014-1030, Jun. 2014.

[15] Z. Wei, C. Zou, F. Leng *et al.*, "Online model identification and state-of-charge estimate for lithium-ion battery with a recursive total least squares-based observer," *IEEE Transactions on Industrial Electronics*, vol. 65, no. 2, pp. 1336-1346, Feb. 2018.

[16] L. Maharjan, S. Inoue, H. Akagi *et al.*, "State-of-charge (SOC)-balancing control of a battery energy storage system based on a cascade PWM converter," *IEEE Transactions on Power Electronics*, vol. 24, no. 6, pp. 1628-1636, Jun. 2009.

[17] M. H. K. Tushar, A. W. Zeineddine, and C. Assi, "Demand-side management by regulating charging and discharging of the EV, ESS, and

[18] S. Piller, M. Perrin, and A. Jossen, "Methods for state-of-charge determination and their applications," *Journal of Power Sources*, vol. 96, no. 1, pp. 113-120, Jun. 2001.

[19] Z. Chen, Y. Fu, and C. Mi, "State of charge estimation of lithium-ion batteries in electric drive vehicles using extended Kalman filtering," *IEEE Transactions on Vehicular Technology*, vol. 62, no. 3, pp. 1020-1030, Mar. 2013.

[20] M. Partovibakhsh and G. Liu, "An adaptive unscented Kalman filtering approach for online estimation of model parameters and state-of-charge of lithium-ion batteries for autonomous mobile robots," *IEEE Transactions on Control Systems Technology*, vol. 23, no. 1, pp. 357-363, Jan. 2015.

[21] C. Chen, R. Xiong, and W. Shen, "A lithium-ion battery-in-the-loop approach to test and validate multiscale dual H infinity filters for state-of-charge and capacity estimation," *IEEE Transactions on Power Electronics*, vol. 33, no. 1, pp. 332-342, Jan. 2018.

[22] W. Cai and J. Wang, "Estimation of battery state-of-charge for electric vehicles using an MCMC-based auxiliary particle filter," in *Proceedings of American Control Conference (ACC)*, Boston, USA, Jul. 2016, pp. 4018-4021.

[23] M. A. Hannan, M. S. H. Lipu, A. Hussain *et al.*, "Neural network approach for estimating state of charge of lithium-ion battery using backtracking search algorithm," *IEEE Access*, vol. 6, pp. 10069-10079, Jan. 2018.

[24] F. Feng, S. Teng, K. Liu *et al.*, "Co-estimation of lithium-ion battery state of charge and state of temperature based on a hybrid electrochemical-thermal-neural-network model," *Journal of Power Sources*, vol. 455, p. 227935, Apr. 2020.

[25] J. C. Á. Antón, P. J. G. Nieto, C. B. Viejo *et al.*, "Support vector machines used to estimate the battery state of charge," *IEEE Transactions on Power Electronics*, vol. 28, no. 12, pp. 5919-5926, Dec. 2013.

[26] M. Charkhgard and M. Farrokhi, "State-of-charge estimation for lithium-ion batteries using neural networks and EKF," *IEEE Transactions on Industrial Electronics*, vol. 57, no. 12, pp. 4178-4187, Dec. 2010.

[27] K. Liu, C. Zou, K. Li *et al.*, "Charging pattern optimization for lithium-ion batteries with an electrothermal-aging model," *IEEE Transactions on Industrial Informatics*, vol. 14, no. 12, pp. 5463-5474, Dec. 2018.

[28] Q. Ouyang, Z. Wang, K. Liu *et al.*, "Optimal charging control for lithium-ion battery packs: a distributed average tracking approach," *IEEE Transactions on Industrial Informatics*, vol. 16, no. 5, pp. 3430-3438, May 2020.

[29] D. Rosewater, R. Baldick, and S. Santoso, "Risk-averse model predictive control design for battery energy storage systems," *IEEE Transactions on Smart Grid*, vol. 11, no. 3, pp. 2014-2022, May 2020.

[30] W. Cao and H. Wang, "An improved corrective security constrained OPF with distributed energy storage," *IEEE Transactions on Power Systems*, vol. 31, no. 2, pp. 1537-1545, Mar. 2016.

[31] N. Padmanabhan, M. Ahmed, and K. Bhattacharya, "Battery energy storage systems in energy and reserve markets," *IEEE Transactions on Power Systems*, vol. 35, no. 1, pp. 215-226, Jan. 2020.

[32] Y. Lin and A. Abur, "A highly efficient bad data identification approach for very large scale power systems," *IEEE Transactions on Power Systems*, vol. 33, no. 6, pp. 5979-5989, Nov. 2018.

[33] M. Chen and G. A. Rincon-Mora, "Accurate electrical battery model capable of predicting runtime and I-V performance," *IEEE Transactions on Energy Conversion*, vol, 21, no. 2, pp. 504-511, Jun. 2006.

[34] H. Dai, X. Wei, and Z. Sun, "Model based SOC estimation for high-power Li-ion battery packs used on FCHVs," *High Technology Letters*, vol. 13, no. 3, pp. 322-326, Sept. 2007.

[35] A. Hentunen, T. Lehmuspelto, and J. Suomela, "Time-domain parameter extraction method for Thévenin-equivalent circuit battery models," *IEEE Transactions Energy Conversion*, vol. 29, no. 3, pp. 558-566, Sept. 2014.

[36] Q. Song, Y. Mi, and W. Lai, "A novel variable forgetting factor recursive least square algorithm to improve the anti-interference ability of battery model parameters identification," *IEEE Access*, vol. 7, pp. 61548-61557, Mar. 2019.

[37] H. W. Sorenson, "Least-squares estimation: from Gauss to Kalman," *IEEE Spectrum*, vol. 7, no. 7, pp. 63-68, Jul. 1970.

[38] U.S. Energy Information Administration. (2020, Apr.). Battery energy storage in the United States: an update on market trends. [Online]. Available: https://www. eia. gov/analysis/studies/electricity/batterystorage/pdf/battery_storage.pdf

[39] A. Abur and A. Gómez-Expósito, *Power System State Estimation: The-*

ory and Implementation. New York: Marcel Dekker, 2004.

[40] H. He, R. Xiong, X. Zhang *et al.*, "State-of-charge estimation of the lithium-ion battery using an adaptive extended Kalman filter based on an improved Thevenin model," *IEEE Transactions on Vehicular Technology*, vol. 60, no. 4, pp. 1461-1469, May 2011.

[41] F. Sun, X. Hu, Y. Zou *et al.*, "Adaptive unscented Kalman filtering for state of charge estimation of a lithium-ion battery for electric vehicles," *Energy*, vol. 36, no. 5, pp. 3531-3540, May 2011.

[42] K. Liu, Y. Li, X. Hu *et al.*, "Gaussian process regression with automatic relevance determination kernel for calendar aging prediction of lithium-ion batteries," *IEEE Transactions on Industrial Informatics*, vol. 16, no. 6, pp. 3767-3777, Jun. 2020.

[43] K. Liu, X. Hu, Z. Wei *et al.*, "Modified Gaussian process regression models for cyclic capacity prediction of lithium-ion batteries," *IEEE Transactions on Transportation Electrification*, vol. 5, no. 4, pp. 1225-1236, Dec. 2019.

[44] K. Liu, Y. Shang, Q. Ouyang *et al.*, "A data-driven approach with uncertainty quantification for predicting future capacities and remaining useful life of lithium-ion battery," *IEEE Transactions on Industrial Electronics*, vol. 68, no. 4, pp. 3170-3180, Apr. 2021.

[45] Z. Fang, Y. Lin, S. Song *et al.*, "State estimation for situational awareness of active distribution system with photovoltaic power plants," *IEEE Transactions on Smart Grid*, vol. 12, no. 1, pp. 239-250, Jan. 2021.

[46] Y. Chen, Y. Yao, and Y. Lin, "Dynamic state estimation for integrated electricity-gas systems based on Kalman filter," *CSEE Journal of Power and Energy Systems*. doi: 10.17775/CSEEJPES.2020.02050

Shaojian Song received the B.S. and M.S. degrees from Guangxi University, Nanning, China, in 1994 and 2001, respectively. Since 1994, he has been with the School of Electrical Engineering at Guangxi University, where he became a Professor in 2010. He visited New York State Center for Future Energy Systems at Rensselaer Polytechnic Institute, New York, USA, from 2014 to 2015. His current research interests include power electronics and energy conversion, active distribution networks, state estimation, optimal control, and machine learning.

Huangjiao Wei received the B.S. degree in China University of Mining and Technology, Xuzhou, China, in 2017. She received the M.S. degree in control engineering from Guangxi University, Nanning, China, in 2020. Her research interests include new energy integration and state estimation of active distribution systems.

Yuzhang Lin received the bachelor's and master's degrees from Tsinghua University, Beijing, China, in 2012 and 2014, respectively, and the Ph.D. degree from Northeastern University, Boston, USA, in 2018. He is currently an Assistant Professor in the Department of Electrical and Computer Engineering at the University of Massachusetts, Lowell, USA. His research interests include smart grid modeling, monitoring, data analytics, and cyber-physical resilience.

Cheng Wang received the B.Sc. and Ph.D. degrees in electrical engineering from Tsinghua University, Beijing, China, in 2012 and 2017, respectively. He is currently an Associate Professor with North China Electric Power University, Beijing, China. His research interests include operation and control of integrated energy systems.

Antonio Gómez-Expósito is the Endesa Chair Professor at the Department of Electrical Engineering, University of Seville, Seville, Spain, which he chaired for twelve years. He has coauthored over 300 publications, including a dozen textbooks and monographs about Circuit Theory and Power System Analysis. He is a Fellow of the IEEE and past editor of IEEE Transactions on Power Systems. Currently, he serves as Vice Editor-in-Chief of the Journal of Modern Power Systems and Clean Energy. He has received many recognitions such as the IEEE/PES Outstanding Power Engineering Educator Award (2019), the Golden Insignia granted by the Spanish Association for the Development of Electrical Engineering (2013) and the Research and Technology Transfer Award, granted by the Government of Andalusia (2011). His primary areas of interest include optimal power system operation, state estimation, digital signal processing, and control of flexible AC transmission system devices.